Identifiability and Kalman Filter Parameter Estimation Applied to Biomolecular Controller Motifs

Eivind S. Haus, **Malin Harr Overland**, **Damiano Rotondo**, **Kristian Thorsen**, **Tormod Drengstig**

Department of Electrical Engineering and Computer Science, University of Stavanger, Norway, (eivind.haus@uis.no)

Abstract: In this paper we apply Augmented Extended Kalman filters (AEKFs) to perform parameter estimation in two different biological controller motifs under both noise-free and noisy conditions. Based on measurements of the two states of the controller motifs, we show that under both noise conditions it is possible to estimate all 5 and 6 parameters, respectively, which is in accordance with previously published results that investigated the theoretical concept of *structural identifiability*. We further investigate how the level of process/measurement noise and the initial estimates of both the parameters and states in the AEKFs affect the estimation performance, and the results indicate that the degree of non-linearity affects filter performance.

Keywords: controller motifs, observability, identifiability, Augmented Extended Kalman filter

1. INTRODUCTION

Mathematical models are widely used to understand and predict the behavior of real-world systems, both human-engineered and natural. Within the field of systems biology, complex models of metabolic pathways and entire cells have been created in recent years. In this context, *controller motifs* are simple biomolecular reaction networks that can explain how regulatory function is achieved through negative feedback, see e.g. Thorsen et al. (2013); Briat et al. (2016); Tang and McMillen (2016), and thus, they are useful as building blocks in larger biological models as shown in Agafonov et al. (2016).

One of the main purposes of a mathematical model is to make predictions of the modeled system's behavior. The accuracy of model predictions is heavily reliant on parameter values, and finding accurate parameter values is often a difficult and time-consuming process that requires experiments. *Identifiability* and *observability* are two closely related concepts that are helpful tools when evaluating the usefulness of a model, as they provide information on whether the model can be parameterized with the available measurements. Identifiability describes whether unknown model parameters can be determined based on knowledge of the input and output of the model. On the other hand, observability implies that it is possible to infer the values of unmeasured states by combining together the measurements and the available model.

In practice, the estimation of unmeasured states is achieved by designing a special type of dynamical system called *state observer*. Among several possible structures proposed for models described by nonlinear differential equations, the extended Kalman filter (EKF) is the *de facto* standard in many applications, such as navigation systems and GPS, see e.g. Huang et al. (2009); Loron and Laliberte (1993); Böhler et al. (2021); Narayanan et al. (2020). The EKF merges two sources of information: the mathematical model, used to compute future prediction of the state based on the current estimate, and the measurements, which introduce a feedback mechanism for addressing possible model-reality mismatch and the presence of unmodeled disturbances. This information fusion is done by weighting the different sources of information according to their reliability (for example, a noisy measurement is weighted less than the data coming from a precise sensor). The EKF addresses the inherent nonlinearities of the model by applying a linearization based on first-order Taylor expansions, thus approximating the nonlinearities as linear functions in small regions around the current state estimate. Although this linearization introduces some error, motivating the search for more efficient estimators (see, e.g., Julier and Uhlmann (1997); Huang et al. (2020); Sarmavuori and Sarkka (2011); Liu and Guo (2021); Rotondo (2023)), the EKF is still considered to be effective in many practical scenarios.

In Haus et al. (2023), the *structural identifiability* of a set of controller motifs was investigated using a symbolic approach. Structural identifiability is a theoretical concept that is fully determined by the structure of the model and the chosen outputs, and assumes that measurements are noise-free and sufficiently informative, see e.g. Ljung and Glad (1994); Villaverde et al. (2018). As it is well known that available measurements from biological systems are limited, practical identifiability limitations may occur for models that have been found to be structurally identifiable. In this paper, we investigate identifiability of controller motifs in a practical setting using Augmented Extended Kalman filters (AEKFs) with varying degree of process/measurement noise. We further investigate how the initial conditions of the parameters and state variables in the filters affect the performance.

2. CONTROLLER MOTIFS

Controller motifs are simple molecular reaction networks where negative feedback is achieved through signaling between the species. In this paper, we consider motif 1 and 3, shown in Fig. 1, from the set of 8 basic two component controller motifs presented in Drengstig et al. (2012).

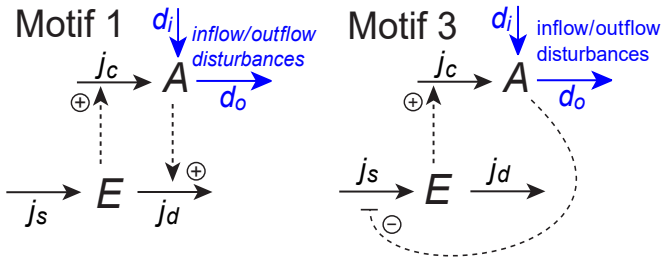

Fig. 1. Basic controller motif 1 and 3.

The general state equations for the motifs are given as:

$$\dot{A}(t) = d_i(t) - d_o(t) + j_c(t) \tag{1}$$

$$\dot{E}(t) = j_s(t) - j_d(t), \tag{2}$$

where A is the controlled species, E is the controller species, d_i and d_o are input and output disturbances, respectively, j_c is the compensatory flow, and j_s and j_d are the synthesis and degradation flows of E, respectively.

The purpose of the compensatory flow j_c is to maintain the level of A by adding A in the presence of a dominating outflow disturbance d_o, and both motifs are therefore called *inflow* controllers. Moreover, j_c is for both motifs *activated* by E as increased level of E results in increased inflow through j_c (indicated by a $\oplus$ sign). The difference between the two motifs is the signaling from A to E, where motif 1 is activating and motif 3 is inhibiting (higher level of A results in lesser flow). We assume that activation is modeled as first order kinetics and inhibition as saturable kinetics. Furthermore, inflows (synthesis) are modeled as zero order, while outflows (degradation) are modeled as first order with respect to its own state variable. The state equations for motifs 1 and 3 are given in Eqs. (3)–(6):

Motif 1:

$$\dot{A}(t) = k_i - k_o{\cdot}A(t) + k_c{\cdot}E(t) \tag{3}$$

$$\dot{E}(t) = k_s - k_d{\cdot}A(t){\cdot}E(t), \tag{4}$$

Motif 3:

$$\dot{A}(t) = k_i - k_o{\cdot}A(t) + k_c{\cdot}E(t) \tag{5}$$

$$\dot{E}(t) = k_s{\cdot}\frac{K_i^A}{K_i^A + A(t)} - k_d{\cdot}E(t), \tag{6}$$

where k_i, k_o, k_c, k_s, and k_d are rate constants, and K_i^A is an inhibition constant.

3. OBSERVABILITY AND IDENTIFIABILITY

In order to introduce the concepts of observability and identifiability we consider a general nonlinear state space model:

$$\dot{x}(t) = f(x(t), p, u(t)) \tag{7}$$

$$y(t) = g(x(t), p) + v(t) \tag{8}$$

$$x_0 = x(t_0, p), \tag{9}$$

where $x(t)\in\mathbb{R}^{n_x}$ is the state vector, $u(t)\in\mathbb{R}^{n_u}$ is the input vector, $y(t)\in\mathbb{R}^{n_y}$ is the output vector, $v(t)\in\mathbb{R}^{n_y}$ is the measurement noise vector, and $p\in\mathbb{R}^{n_p}$ is a vector of system parameters assumed to be constant. Furthermore, $x_0\in\mathbb{R}^{n_x}$ denotes the initial conditions, and the nonlinear functions $f(\cdot)$ and $g(\cdot)$ define the state and output equation, respectively.

3.1 Observability

Biological systems are typically only partially observable due to experimental limitations, and the available system outputs may be a function of several states and/or parameters (Raue et al., 2009). Thus, to determine the unmeasurable states they must be be inferred from the available system outputs, which is possible only if the system is *observable* (Kalman, 1960).

"Observability: Given an initial state x_0 and an admissible control $u(t)$, if the current system state $x(t)$ can be determined only through the system output $y(t)$ in a finite time, the system is said to be observable. (Miao et al., 2011)"

Observability is a theoretical concept determined by the system structure and the chosen outputs and typically assumes noise-free measurements of the system output y and that the parameters p of the model are known. However, the parameters of a biological system are rarely known, as these typically represent biochemical processes inside the cells that are impossible to measure directly. Thus, the parameter values must be estimated, typically based on experiments, which often is associated with high cost. In order to minimize the potential cost of experiments, *identifiability* analysis is a useful tool in finding which measurements are necessary to fully parameterize a model.

3.2 Identifiability

Identifiability: The dynamic system given by Eqs. (7)–(9) is identifiable if p can be uniquely determined from the given system input $u(t)$ and the measurable system output $y(t)$; otherwise, it is said to be unidentifiable, (Miao et al., 2011).

If a model is identifiable, it is possible to uniquely determine the value of all its system parameters based on the chosen model structure and outputs. Thus, through performing identifiability analysis for different measurement combinations, the smallest, or easiest to perform, set of measurements that allows the model to be accurately parameterized can be found. However, identifiability is, as observability, a theoretical concept, and *practical* identifiability limitations such as noisy measurements, restrictions on admissible inputs, or limited time resolution of outputs may occur.

Observability and identifiability both imply a strong connection between inputs, states and outputs, and identifiability can be considered a particular case of observability where system parameters are treated as states with zero dynamics, see e.g. Villaverde et al. (2016); Villaverde (2019). Consequently, the parameters p are included as part of the state vector x and methods originally developed for investigating observability can also be used for parameter identifiability as shown in Villaverde et al. (2016). This

approach is similar to an Augmented Kalman filter, which we introduce in the next section.

4. KALMAN FILTERING

Let us consider the discrete-time nonlinear system:

$$z(k+1) = \phi\left(z(k), u(k)\right) + w(k) \tag{10}$$
$$y(k) = \gamma\left(z(k)\right) + v(k) \tag{11}$$

where $z(k)\in\mathbb{R}^{n_z}$ denotes the (unknown) state vector, $u(k)\in\mathbb{R}^{n_u}$ denotes the (known) input vector, $y(k)\in\mathbb{R}^{n_y}$ denotes the (known) output vector, $w(k)\in\mathbb{R}^{n_x}$ is the (unknown) process noise, $v(k)\in\mathbb{R}^{n_v}$ is the (unknown) measurement noise, and $\phi(\cdot)$ and $\gamma(\cdot)$ denote known functions assumed to be differentiable with respect to z. It is also assumed that $w(k)$ and $v(k)$ are zero mean multivariate Gaussian noise with (known) covariance matrices $Q\in\mathbb{S}^{n_z}$ and $R\in\mathbb{S}^{n_h}$, respectively, where $\mathbb{S}^n$ denotes (real) symmetric matrices of order n.

4.1 Extended Kalman filter (EKF)

The EKF comprises alternating phases of model-based prediction and measurement-based update, forming an ongoing (theoretically infinite) cycle involving the following variables and matrices, which are internal to the EKF:

- the *a priori estimate* $\bar{z}(k)\in\mathbb{R}^{n_z}$;
- the *a priori covariance matrix* $M(k) = E\left[\left(z(k)-\bar{z}(k)\right)\left(z(k)-\bar{z}(k)\right)^T\right]\in\mathbb{S}^{n_z}$;
- the *a posteriori estimate* $\hat{z}(k)\in\mathbb{R}^{n_z}$;
- the *a posteriori covariance matrix* $P(k) = E\left[\left(z(k)-\hat{z}(k)\right)\left(z(k)-\hat{z}(k)\right)^T\right]\in\mathbb{S}^{n_z}$;

During the model-based prediction, the EKF computes the *a priori estimate* based on the state equation, as follows:

$$\bar{z}(k) = \phi\left(\hat{z}(k-1), u(k-1)\right) \tag{12}$$

At the same time, the *a priori covariance matrix* is updated according to the following equation:

$$M(k) = \mathcal{A}(k)P(k-1)\mathcal{A}(k)^T + Q \tag{13}$$

where the matrix $\mathcal{A}(k)$ is obtained through a first-order Taylor approximation of the nonlinear function ϕ at the most recent state estimate:

$$\mathcal{A}(k) = \left.\frac{\partial\phi}{\partial z}\right|_{\hat{z}(k-1),u(k-1)} \tag{14}$$

where the operator ∂/∂ is meant in the Jacobian matrix sense.

During the measurement-based update, the EKF computes the Kalman gain $K(k)$ to be used to account for the so-called *innovation*, i.e., the measurement-estimate mismatch, according to:

$$K(k) = M(k)\mathcal{C}(k)^T\left[\mathcal{C}(k)M(k)\mathcal{C}(k)^T + R\right]^{-1} \tag{15}$$

where the matrix $\mathcal{C}(k)$ is obtained through a first-order Taylor approximation of the nonlinear function γ at the most recent state estimate:

$$\mathcal{C}(k) = \left.\frac{\partial\gamma}{\partial z}\right|_{\bar{z}(k)} \tag{16}$$

The Kalman gain essentially determines how much weight is given to the current measurement, and helps strike a balance between trusting the model and incorporating new measurements $y(k)$, according to the following equation:

$$\hat{z}(k) = \bar{z}(k) + K(k)\left[y(k) - \gamma\left(\bar{z}(k)\right)\right] \tag{17}$$

Finally, the current value of the a posteriori covariance matrix is computed using:

$$P(k) = \left[I - K(k)\mathcal{C}(k)\right]M(k) \tag{18}$$

4.2 Augmented Extended Kalman filter (AEKF)

Following an approach that is well consolidated in the field of fault diagnosis, see e.g. Patton and Klinkhieo (2009); Zhang et al. (2020); Rotondo et al. (2021), it is possible to use state observers, such as the above described EKF, to obtain a real-time estimate of the unknown parameter vector p appearing in Eq. (7). The first required step is a discretization of Eq. (7), which can be done using a variety of methods (Franklin et al., 1998), with forward-Euler being the most common due to its simplicity, thus obtaining:

$$x(k+1) = x(k) + T_s\cdot f(x(k), p, u(k)) \tag{19}$$
$$y(k) = g(x(k), p) + v(k) \tag{20}$$
$$x_0 = x(k_0, p), \tag{21}$$

where T_s denotes the sampling time. Then, a description of the dynamical behavior of the parameters to be estimated is introduced, which in the case of constant parameters reads as follows:

$$p(k+1) = p(k) \tag{22}$$

At this point, it is possible to define an augmented state vector as $z(k) = \left[x(k)^T, p(k)^T\right]^T = \left[z_1(k)^T, z_2(k)^T\right]^T$ and, by combining together Eqs. (19)–(22), obtain an augmented state-space model that fits the form of Eqs. (10)–(11), with:

$$\phi\left(z(k), u(k)\right) = \begin{bmatrix} z_1(k) + f\left(z_1(k), z_2(k), u(k)\right) \\ z_2(k) \end{bmatrix} \tag{23}$$
$$\gamma\left(z(k)\right) = g\left(z_1(k), z_2(k)\right) \tag{24}$$

Clearly, an EKF implemented on the augmented model would return estimates $\bar{z}(k)$ and $\hat{z}(k)$ which correspond to the joint state-parameter estimates $\bar{x}(k)$, $\bar{p}(k)$ and $\hat{x}(k)$, $\hat{p}(k)$, respectively.

To this end, one can define the matrix Q to account for disturbances acting on the state x, the possible time-varyingness of p, or to incorporate information about the model uncertainty into the estimation.

4.3 Implementation

The models in Eqs. (3)–(4) and Eqs. (5)–(6), respectively, are the basis for both the process and the AEKF for motif 1 and 3, where the augmented state vectors are given as

$$\text{motif 1:}\quad z(k) = [A, E, k_i, k_o, k_c, k_s, k_d] \tag{25}$$
$$\text{motif 3:}\quad z(k) = [A, E, k_i, k_o, k_c, k_s, k_d, K_i^A]. \tag{26}$$

For easier reference to the parameters, we refer to them as

$$[k_i, k_o, k_c, k_s, k_d, K_i^A] = [k_1, k_2, k_3, k_4, k_5, k_6], \tag{27}$$

or generally as $k_n\forall\ n\in\{1,\dots,N\}$ where N=5 for motif 1 and N=6 for motif 3. As there is no external input $u(k)$, the motifs are *autonomous* systems (Haus et al., 2023), and the estimation is solely based on measurements of the state variables.

5. RESULTS

One of the main findings in Haus et al. (2023) was that noise free measurements of the state variables A and E of motif 1 and 3 proved sufficient for structural identifiability, i.e. in theory it is possible to uniquely estimate all the parameters. Hence, the results presented here are focused on reproducing these results using AEKF, and also to investigate the robustness with respect to noise level and initial filter conditions of parameters and state variables.

5.1 Simulation setup

For simplicity, the values of all the parameters in the process are set to 1, and we term these parameters as $k_{n,\text{process}}$. The steady state values of A and E for each motif are calculated using Eqs. (3)–(4) and Eqs. (5)–(6), respectively. As there are no external input to provide excitation, the initial conditions of A and E in both the process and the AEKF are increased with 30% from the calculated steady state values. The initial conditions of the unknown parameters in the AEKF are assigned a uniformly distributed random number within 1% deviation from the value of $k_{n,\text{process}}$=1. This small deviation is considered sufficient to demonstrate whether the AEKF produce similar results as the structural identifiability from Haus et al. (2023).

For the noisy conditions, both the process noise $w(k)$ and the measurement noise $v(k)$ are modeled as bandwidth limited zero mean white noise. Simulations are run for 10 seconds with a stepsize of T_s=0.0002 seconds. As the AEKFs typically converge within 2 seconds, only the first 3 seconds are shown in Figs. 2–4. In order to quantitatively compare the Kalman filter performances, we calculate the following *parameter error measure* for each individual parameter k_n,

$$\Delta e_n = \frac{1}{5000} \sum_{i=45000}^{50000} \left| k_{n,\text{process}}(i) - k_{n,\text{est}}(i) \right| \qquad (28)$$

where $k_{n,\text{est}}$ is the estimated parameter value. Thus, Δe_n is the mean of the difference between the process value and the estimated value of parameter k_n during the last second of the simulation, i.e. the last 5000 samples. To get a performance measure for the entire motif, we calculate an *overall motif error measure* as follows,

$$\Delta e_{\text{motif}} = \frac{1}{N} \sum_{n=1}^{N} \Delta e_n \qquad (29)$$

where N=5 for motif 1 and N=6 for motif 3.

All state and parameter values are either in arbitrary units or without units.

5.2 Motif 1

The simulation results for the noise free motif 1 are shown in Fig. 2, where we observe that all parameters quickly converge with an overall *motif error measure* of Δe_{motif}=0.0002. These results are in accordance with the findings in Haus et al. (2023). In order to investigate the effect of noise, we added both process and measurement noise to A and E, and increased the noise power gradually. A simulation example of this is shown in Fig. 3, where the

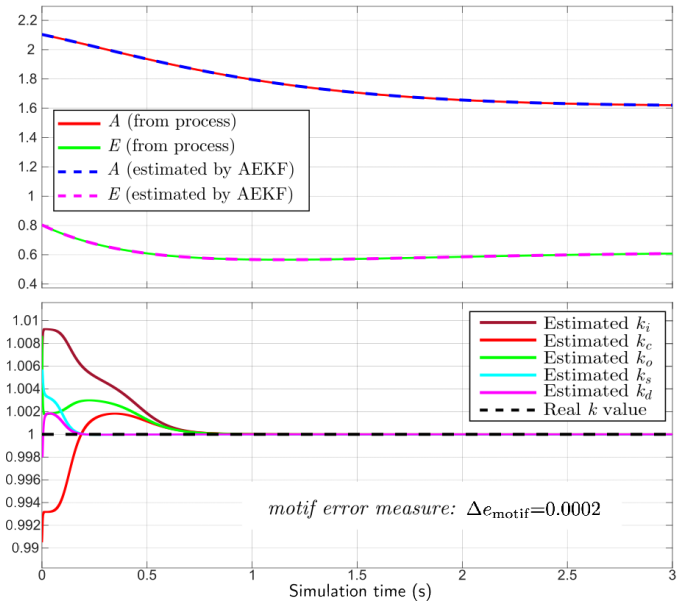

Fig. 2. Simulation results for motif 1 with no noise. The upper panel shows the states A and E, whereas the lower panel shows the parameter estimates.

noise power is $1{\cdot}10^{-6}$ for both $w(k)$ and $v(k)$, and where all parameters converge fairly quickly with an overall *motif error measure* of Δe_{motif}=0.059.

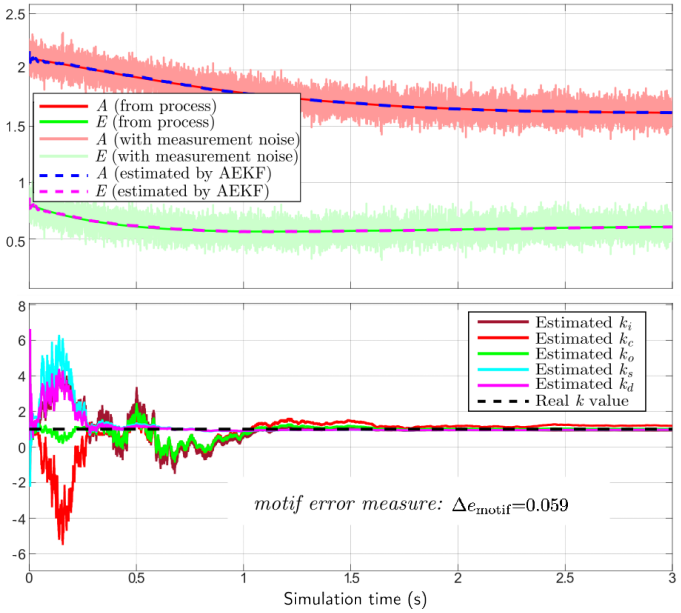

Fig. 3. Simulation results for motif 1 with process and measurement noise. The upper panel shows the states A and E, whereas the lower panel shows the parameter estimates.

The upper panel of Fig. 3 shows that the noise is quite substantial, whereas the lower panel demonstrate that even though several parameters deviate up to 500% from the initial condition during the first 0.5 seconds, all parameters still converge to within 10% of the process value at steady state. Note that negative parameter values implies that the species flow in the motif is reversed. To summarize, we

conclude that the AEKF for motif 1 is quite robust against process and measurement noise.

5.3 Motif 3

Similarly to motif 1, we performed simulations with and without noise for motif 3. The noise free simulations (not shown) revealed slightly slower dynamics compared to motif 1, but with the same overall *motif error measure* of Δe_{motif}=0.0002. On the other hand, when both process noise and measurement noise were added, the AEKF showed poor performance already at a noise power level of $1{\cdot}10^{-11}$, and estimation breaks down at a noise power of $1{\cdot}10^{-10}$ with an overall *motif error measure* of Δe_{motif}=0.5, see Fig. 4. Thus, the AEKF is more sensitive to noise for motif 3 compared to motif 1, and we attribute this to the increased non-linearity from the saturable inhibition term $\frac{K_i^A}{K_i^A+A}$ in Eq. (6).

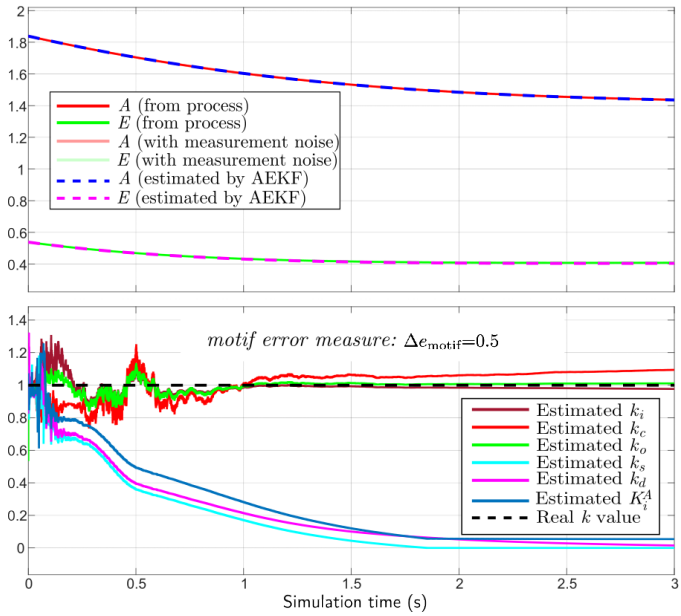

Fig. 4. Simulation results for motif 3 with process and measurement noise. The upper panel shows the states A and E, whereas the lower panel shows the parameter estimates.

5.4 Noise and initial condition of parameters

To investigate the effect of noise in the performance of the AEKF in more detail, we simulated both motifs while the noise power level was increased from $1{\cdot}10^{-15}$ to $1{\cdot}10^{-3}$, in steps of factor 10. To compensate for the randomly chosen initial conditions for the parameters (still within 1% deviation of $k_{n,process}$), we averaged the results over 10 simulations for each noise power value. We performed simulations with *i*) only process noise, *ii*) only measurement noise, and *iii*) both types of noise. As it turned out that the results were more or less similar for all three cases, we present in Fig. 5 the results for case *iii*) only.

Panels A and B show the *averaged parameter error measure* for motif 1 and 3, respectively, calculated as

$$\overline{\Delta e_n} = \frac{1}{10}\sum_{i=1}^{10} \Delta e_{n,i} \tag{30}$$

where $\Delta e_{n,i}\ \forall\ i{\in}1,\ldots,10$ is based on the *parameter error measure* from Eq. (28) calculated during the 10 simulations. The results clearly show that motif 3 is more sensitive to noise than motif 1. Moreover, the profile of each $\overline{\Delta e_n}$ curve (for each parameter) is more consistent for motif 1, whereas the profiles for motif 3 are more diverse where we see that the parameters k_s, k_d, and K_i^A are more prone to low noise levels, while k_c and k_o are more prone to high noise levels.

We also investigated how the initial conditions of the parameter values in the AEKF affected the overall *motif error measure* Δe_{motif} from Eq. (29) in noise free simulations. Thus, we performed simulations where the initial condition for each parameter k_n in the AEKF were increased in steps from the true value of 1 up to 10. These results are shown in panels C and D in Fig. 5 for motif 1 and motif 3, respectively, and we see that the AEKF for motif 1 is relatively unaffected by the increasing initial conditions. Actually, an initial condition 10 times the real parameter value results in $\Delta e_n{\approx}10^{-2}$ for most of the parameters. Interestingly, the curve for parameter k_c have a surprisingly odd shape where Δe_n have a distinct decreased value for an initial condition of 5 times the real parameter value. On the other hand, and in accordance with panel B, the results for motif 3 show relatively poor performance for increased initial conditions. The performance drops significantly already at a small deviation of only a few percent from the real value and becomes increasingly worse as the initial conditions increase.

To summarize, the AEKF show better performance for motif 1 compared to motif 3, both for increasing noise levels and increasing initial conditions for the parameters. The cause of this is likely that motif 3 is more non-linear than motif 1, as although the added noise is initially zero-mean white noise, it is not guaranteed to be zero-mean after being processed through the nonlinear system. Thus, the noise creates a bias which increases with the degree of non-linearity. Furthermore, as the AEKF use a linearized $\mathcal{A}(k)$ matrix based on the current state estimate together with the parameter values with initial conditions far away from the real values, it is most likely to introduce a bias which the Kalman filter is unable to compensate for.

5.5 Initial conditions of A and E

Finally, we examined how the level of excitation of the process affected the performance of the AEKF, i.e. the level of the initial conditions of the states A and E in both the process and the filter. We adjusted the initial conditions for both states simultaneously with a factor α between $0.2{<}\alpha{<}2$, and simulated both without noise and with a noise power of $1{\cdot}10^{-6}$ in both the process and measurement noise. The results are shown in Fig. 6 for motif 1, where Δe_{motif} is plotted as a function of α for both noise free and noisy conditions.

The blue curve in Fig. 6 show that under noise-free conditions only a small excitation in the initial conditions of A and E is necessary to reduce the value of Δe_{motif}.

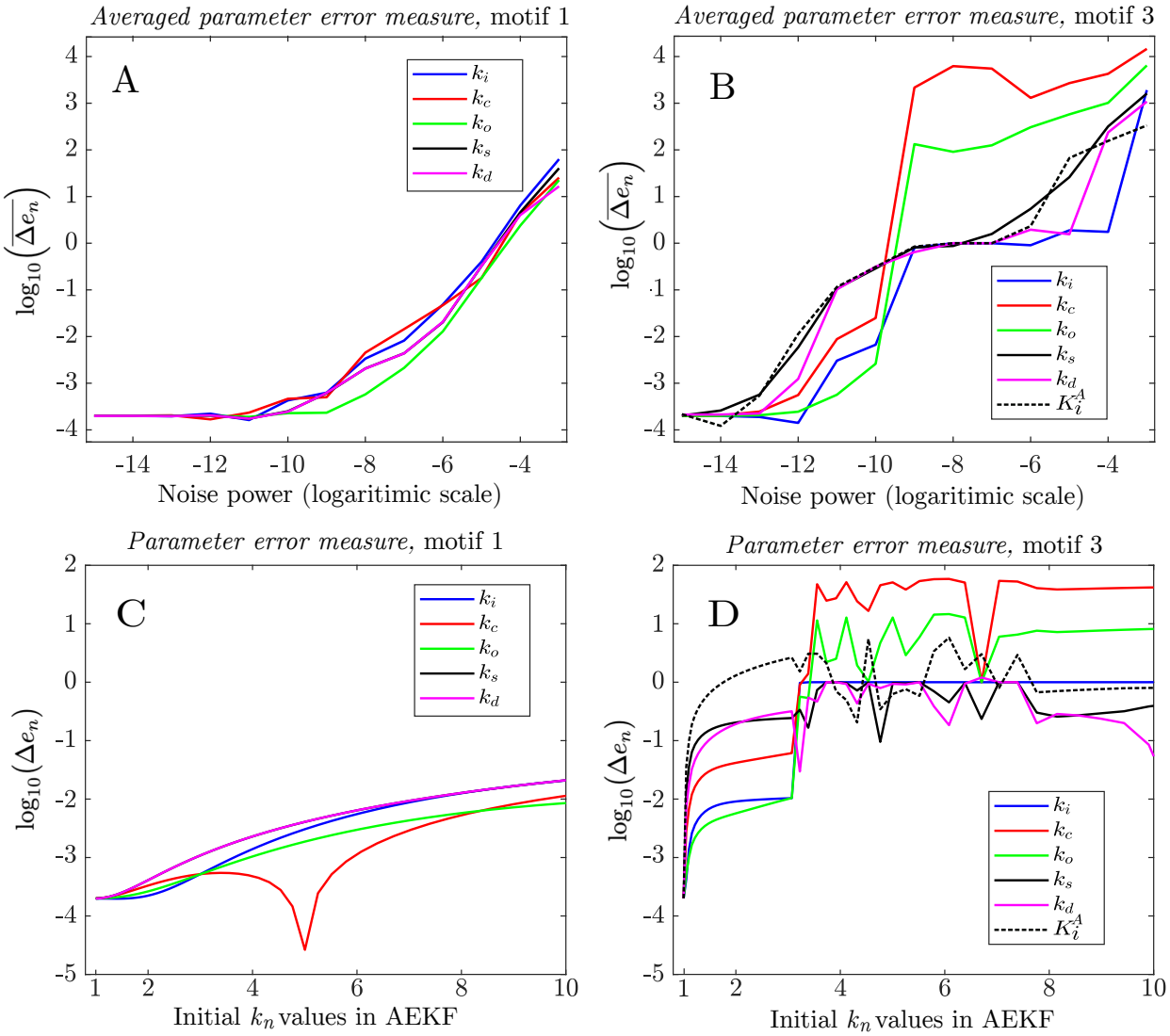

Fig. 5. Panels A/B show the *averaged parameter error measure* $\overline{\Delta e_n}$ from Eq. (30) as a function of noise power for motif 1 / motif 3. Panels C/D show the *parameter error measure* Δe_n from Eq. (28) as a function of initial conditions for the parameters in the AEKFs for motif 1 / motif 3.

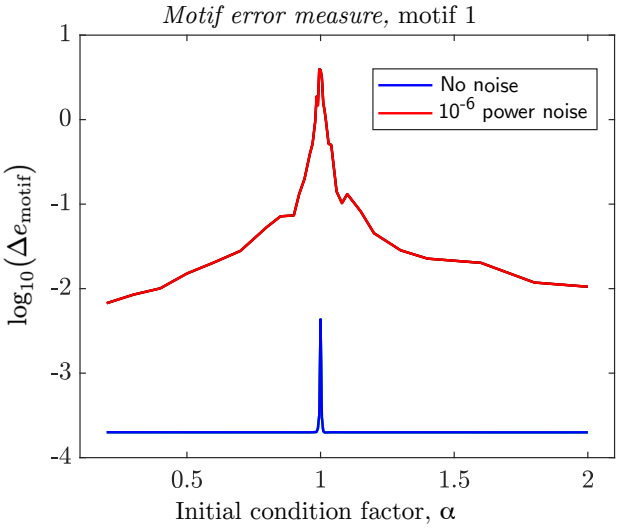

Fig. 6. Plot of the overall *motif error measure* Δe_{motif} as a function of initial condition factor α for both noise free and noisy conditions.

In fact, an increase in α from α=1 to α=1.02 reduces Δe_{motif} from 0.007 to approximately 0.0002. The noisy situation illustrated by the red curve show the same underlying mechanisms where increased excitation in initial conditions of A and E reduces the value of Δe_{motif}, but the decrease is not as prominent and the overall level is higher than for the noise free situation. The results are reasonable since decreased excitation decreases the dynamics of A and E, leading to an increased noise-to-signal ratio. Thus, at low degrees of excitation the information provided to the Kalman filter by the measurements is predominantly noise.

6. CONCLUSIONS

We have implemented an Augmented and Extended Kalman filter (AEKF) able to estimate all unknown parameters for the basic controller motifs 1 and 3 when both states are measured. Under noise free conditions all the parameters were accurately estimated, which corresponds well with previous results showing that these motifs are structurally identifiable with the same measurements. We

also investigated the performance of the AEKF with respect to noise in both the process and measurements, initial conditions of the unknown parameters of AEKF, and finally, the initial conditions of the states A and E. We found that the Kalman filter generally performed better on motif 1 than on the more nonlinear motif 3. This suggests that a state observer better suited for nonlinear models, such as the *Unscented Kalman Filter* (Julier and Uhlmann, 1997), may be more appropriate to use for the more nonlinear controller motifs.

REFERENCES

Agafonov, O., Selstø, C.H., Thorsen, K., Xu, X.M., Drengstig, T., and Ruoff, P. (2016). The Organization of Controller Motifs Leading to Robust Plant Iron Homeostasis. *PLoS ONE*, 11(1), e0147120.

Böhler, L., Ritzberger, D., Hametner, C., and Jakubek, S. (2021). Constrained extended kalman filter design and application for on-line state estimation of high-order polymer electrolyte membrane fuel cell systems. *international journal of hydrogen energy*, 46(35), 18604–18614.

Briat, C., Gupta, A., and Khammash, M. (2016). Antithetic Integral Feedback Ensures Robust Perfect Adaptation in Noisy Bimolecular Networks. *Cell Systems*, 2(1), 15–26.

Drengstig, T., Jolma, I.W., Ni, X.Y., Thorsen, K., Xu, X.M., and Ruoff, P. (2012). A Basic Set of Homeostatic Controller Motifs. *Biophysical Journal*, 103(9), 2000–2010.

Franklin, G.F., Powell, J.D., Workman, M.L. (1998). *Digital control of dynamic systems*, Third edition, Addison-Wesley Reading, MA.

Haus, E.S., Drengstig, T., and Thorsen, K. (2023). Structural identifiability of biomolecular controller motifs with and without flow measurements as model output. *PLoS Computational Biology*, 19(8), e1011398.

Huang, Y., Zhu, F., Jia, G., and Zhang, Y. (2020). A slide window variational adaptive Kalman filter. *IEEE Transactions on Circuits and Systems II: Express Briefs*, 67(12), 3552–3556.

Huang, Z., Du, P., Kosterev, D., and Yang, B. (2009). Application of extended kalman filter techniques for dynamic model parameter calibration. In *2009 IEEE Power & Energy Society General Meeting*, 1–8. IEEE.

Julier, S.J. and Uhlmann, J.K. (1997). New extension of the Kalman filter to nonlinear systems. In *Signal processing, sensor fusion, and target recognition VI*, volume 3068, 182–193. Spie.

Kalman, R. (1960). On the General Theory of Control Systems. *IFAC Proceedings Volumes*, 1(1), 491–502.

Liu, J. and Guo, G. (2021). Vehicle localization during GPS outages with extended Kalman filter and deep learning. *IEEE Transactions on Instrumentation and Measurement*, 70, 1–10.

Ljung, L. and Glad, T. (1994). On global identifiability for arbitrary model parametrizations. *Automatica*, 30(2), 265–276.

Loron, L. and Laliberte, G. (1993). Application of the extended kalman filter to parameters estimation of induction motors. In *1993 Fifth European Conference on Power Electronics and Applications*, 85–90. IET.

Miao, H., Xia, X., Perelson, A.S., and Wu, H. (2011). On Identifiability of Nonlinear ODE Models and Applications in Viral Dynamics. *SIAM Review*, 53(1), 3–39.

Narayanan, H., Behle, L., Luna, M.F., Sokolov, M., Guillén-Gosálbez, G., Morbidelli, M., and Butté, A. (2020). Hybrid-ekf: Hybrid model coupled with extended kalman filter for real-time monitoring and control of mammalian cell culture. *Biotechnology and Bioengineering*, 117(9), 2703–2714.

Patton, R.J. and Klinkhieo, S. (2009). Actuator fault estimation and compensation based on an augmented state observer approach. In *Proceedings of the 48h IEEE Conference on Decision and Control (CDC) held jointly with 2009 28th Chinese Control Conference*, 8482–8487. IEEE.

Raue, A., Kreutz, C., Maiwald, T., Bachmann, J., Schilling, M., Klingmüller, U., and Timmer, J. (2009). Structural and practical identifiability analysis of partially observed dynamical models by exploiting the profile likelihood. *Bioinformatics*, 25(15), 1923–1929.

Rotondo, D. (2023). The Weighted Kalman Filter. *IFAC-PapersOnLine*, 56(2), 8869–8874.

Rotondo, D., Buciakowski, M., and Witczak, M. (2021). Simultaneous state and process fault estimation in linear parameter varying systems using robust quadratic parameter varying observers. *International Journal of Robust and Nonlinear Control*, 31(17), 8390–8407.

Sarmavuori, J. and Sarkka, S. (2011). Fourier-hermite Kalman filter. *IEEE Transactions on Automatic Control*, 57(6), 1511–1515.

Tang, Z.F. and McMillen, D.R. (2016). Design principles for the analysis and construction of robustly homeostatic biological networks. *Journal of Theoretical Biology*, 408, 274–289.

Thorsen, K., Ruoff, P., and Drengstig, T. (2013). Control theoretic properties of physiological controller motifs. *ICSSE 2013 - IEEE International Conference on System Science and Engineering, Proceedings*, 165–170.

Villaverde, A.F. (2019). Observability and Structural Identifiability of Nonlinear Biological Systems. *Complexity*, 2019.

Villaverde, A.F., Barreiro, A., and Papachristodoulou, A. (2016). Structural Identifiability of Dynamic Systems Biology Models. *PLoS Computational Biology*, 12(10), e1005153.

Villaverde, A.F., Evans, N.D., Chappell, M.J., and Banga, J.R. (2018). Sufficiently Exciting Inputs for Structurally Identifiable Systems Biology Models. *IFAC-PapersOnLine*, 51(19), 16–19.

Zhang, W., Wang, Z., Raïssi, T., Wang, Y., and Shen, Y. (2020). A state augmentation approach to interval fault estimation for descriptor systems. *European Journal of Control*, 51, 19–29.